Received: 28 April 2023 | Accepted: 27 June 2023

DOI: 10.1002/maco.202313894

ARTICLE

Materials and Corrosion

# Measurements on macrocells made of segmented reinforcement in concrete showing environmental impacts on corrosion of steel in concrete

**Franz Pruckner**

Ingenieurkonsulent für Chemie/Graduated Consulting Engineer for Chemistry/Ingénieur-Conseil de la Chimie, Euratsfeld, Austria

**Correspondence**
Franz Pruckner, Ingenieurkonsulent für Chemie/Graduated Consulting Engineer for Chemistry/Ingénieur-Conseil de la Chimie, AT-3324 Euratsfeld, Austria.
Email: franz.pruckner@betondoktor.com

**Funding information**
None

**Abstract**

Corrosion of steel in concrete can be characterized by measuring the galvanic current density when a macrocell is established. On nonpolarized steel, however, other electrochemical techniques like linear polarization resistance measurements may be used to characterize the electrochemical state of steel in concrete. On existing structures with their large dimensions and local differences in exposure conditions, local differences in the electrochemical state of the embedded reinforcement are established, leading to potential differences along the reinforcement and galvanic currents flowing. When it is possible to isolate anodic areas from the rest of the reinforcement, both galvanic current measurements, determination of polarization resistance on the separated anodic areas and the driving force between the anodic segments and the reinforcement are possible to obtain. In this work, this procedure is discussed and verified on a field structure on anodic areas caused by cracks in the concrete overlay and the results thereof are presented.

KEYWORDS

corrosion current, environmental impact, galvanic current, linear polarization resistance, segmented reinforcement

## 1 | INTRODUCTION

The simplest way to monitor the electrochemical state of the reinforcement is to measure the corrosion potential. Monitoring the potential over time may deliver a change in corrosion activity by that is, chloride ingress. However, potentials fail to provide quantitative information on the corrosion rate of the reinforcement. Various electrochemical techniques have therefore been adopted to measure the corrosion rate of steel in concrete. Handheld instruments have been developed that use mainly the technique of linear polarization resistance (LPR) measurements or galvanostatic pulse measurements to be used in condition surveys. The same electrochemical techniques have also been adopted to be used in combination with permanent embedded sensors so that the change of the corrosion rate of the reinforcement can be monitored over time. This technique applies preferably to steel where only microcell corrosion takes place. In a microcell, anodic and cathodic regions are formed alternately along the surface of the same reinforcement bar in very close proximity to each other. When a macrocell is formed on the steel then the electrochemical techniques for corrosion rate measurements are performed on polarized systems leading to results that cannot easily be interpreted. For such cases, the technique of galvanic current measurements may deliver more valuable information. Macrocells develop due to differences in aeration (oxygen), alkalinity (carbonation), or salt concentration (chloride ingress). For active/

  

passive macrocells, the driving force may amount to several hundreds of millivolts.

In cases where it is possible to isolate segments of active areas from the passive areas of a reinforcement network it is possible to perform various electrochemical techniques to assess information about the corrosion rate both caused by microcell and macrocell corrosion and the measurement values related to each other. It is expected that this will deliver a more precise picture of the corrosion condition.

## 2 | THEORETICAL BACKGROUND

To be able to compare galvanic current densities and corrosion current densities, a simplified galvanic corrosion cell is considered. In this cell,

1. no ohmic potential drop exists in the solution,
2. both oxidation and reduction reactions are activation controlled and the reduction reaction in both metals is the hydrogen evolution reaction,
3. the metal $Me_1$ is more noble than metal $Me_2$ which means

$$E_{corr}(Me_1) < E_{corr}(Me_2),$$

4. the hydrogen evolution reaction is favored on the more noble metal $|i_{0,H_2(Me_1)}| \gg |i_{0,H_2(Me_2)}|$, and
5. the possible anodic reactions are

$$Me_1 \rightarrow Me_1^+ + e^-,$$

$$Me_2 \rightarrow Me_2^+ + e^-.$$

As long as the two dissimilar metals are disconnected (open circuit) each metal will undergo self-corrosion in accordance with the mixed potential theory[1] where the self-corrosion rate is given by

$$I_{corr} = |I_{red}| \text{ for each metal.} \quad (1)$$

The self-corrosion rates can be determined by the intersection of the Tafel slopes for oxidation and reduction reactions separately for each metal thus defining the corrosion potential and corrosion rate for each metal. The difference in the corrosion potential can be considered as the driving force of the galvanic couple for the noble and active metal

$$\Delta U_{circuit} = E_{corr}(Me_2) - E_{corr}(Me_1) \text{ at open circuit.} \quad (2)$$

When closing the circuit the two metals are forced to stabilize at the same potential as long as the ohmic drops in the solution and in the external circuits are negligible

$$E_{galvanic\ couple} = E_{Me_1} = E_{Me_2} \text{ at closed circuit.} \quad (3)$$

At this particular potential, the sum of all oxidation rates needs to be equal to the sum of all reduction rates

$$\sum I_{ox} = \sum |I_{red}|. \quad (4)$$

For the galvanic system presented in Figure 1, Equation (4) can be expanded to

$$I_{corr}(\underline{Me_1} - Me_2) + I_{corr}(Me_1 - \underline{Me_2}) = |I_{H_2}(Me_1)| + |I_{H_2}(Me_2)|, \quad (5)$$

where, $I_{corr}(\underline{Me_1} - Me_2)$ is the corrosion rate of $Me_1$ due to galvanic coupling with $Me_2$, $I_{corr}(Me_1 - \underline{Me_2})$ is the corrosion rate of $Me_2$ due to galvanic coupling with $Me_1$, $|I_{H_2}(Me_1)|$ is the rate of hydrogen evolution on $Me_1$, $|I_{H_2}(Me_2)|$ is the rate of hydrogen evolution on $Me_2$.

In the case that hydrogen evolution on the more noble metal is favored then this equation can be simplified to

$$I_{corr}(Me_1 - \underline{Me_2}) = |I_{H_2}(Me_1)|. \quad (6)$$

However, this corrosion current is not the same as the galvanic current flowing in the closed system. The galvanic current flowing according to Figure 1 is defined as

$$I_{galvanic\ couple} = I_{corr}(Me_1 - \underline{Me_2}) - I_{corr}(Me_2). \quad (7)$$

This fact has to be taken into consideration when comparing corrosion rate measurements on measurement coupons determined by that is, LPR method with galvanic current measurements on the same coupons. For the ideal case described in Figure 1, the galvanic current $I_{galvanic\ couple}$ shall be higher than the corrosion current $I_{corr}(Me_2)$. In practice for a galvanic element established between more and less noble parts of the reinforcement network, the driving force may be so small that the corrosion current exceeds the galvanic current. In cases where the expected anodic segment of the reinforcement turns out to be more cathodic than the rest of the reinforcement network, the galvanic current will turn negative. So, in practice, the following cases should be principally possible

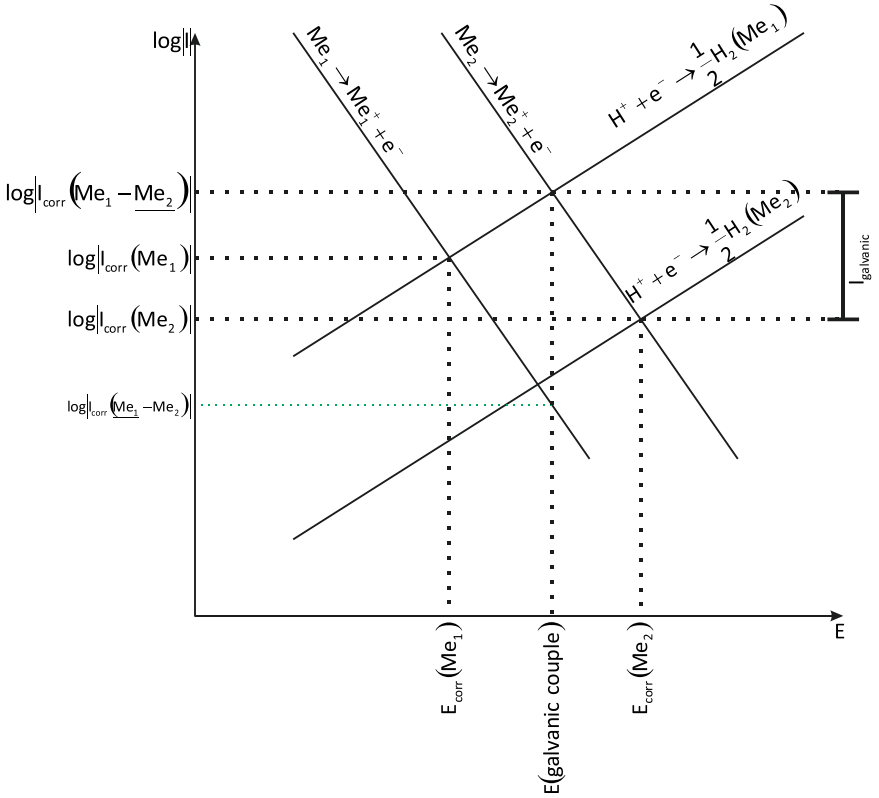


**FIGURE 1** Use of Tafel-plots to determine galvanic corrosion rates.

1. $I_{\text{galvanic couple}} > I_{\text{corr}}(\text{Me}_2)$,
2. $I_{\text{galvanic couple}} < I_{\text{corr}}(\text{Me}_2)$,
3. $I_{\text{galvanic couple}} < 0$.

In addition, the corrosion current density is also dependent on the ambient temperature. Ideally, the corrosion current density increases with temperature showing a linear correlation between the logarithm of $i_{\text{corr}}$, $T$ and the reciprocal temperature (electrochemical Arrhenius plot)

$$i_{\text{corr},T} = i_{\text{corr,298K}} \cdot \exp\left[-\frac{E_{\text{A}}}{R} \cdot \left(\frac{1}{T} - \frac{1}{298\ \text{K}}\right)\right], \quad (8)$$

with $i_{\text{corr,298K}}$, corrosion current density at 298 K, $E_{\text{A}}$, activation energy for the corrosion reaction, Rgas constant (8.3144 J mol$^{-1}$ K$^{-1}$).

The activation energy for the corrosion reaction was found to be in the range of 10–35 kJ/mol. With increasing chloride content, the activation energies are supposed to increase as well.[2–4]

## 3 | SCOPE

The aim of this work is to verify the above-derived theoretical considerations and to quantify the differences in the galvanic corrosion current of a coupon short-circuited with the rebar network and the corrosion current (determined by LPR) of the isolated segment of the reinforcement.

It is also of interest to determine the driving force of the galvanic couple and the development of these three parameters with time to quantify the environmental influence to the development of a corrosion cell on a reinforcement network.

## 4 | EXPERIMENTAL

### 4.1 | Measurement setup

All measurements are performed on a real structure. The structure is a subterranean car park in the south western part of Germany. The installation was performed when the structure was approximately 10 years old. The basic idea was to monitor corrosion rate/corrosion risk of the reinforcement with time in areas where the overlay concrete developed cracks and how environmental impacts are influencing the corrosion risk/corrosion rate of the same reinforcement segments.

From the existing reinforcement network consisting of Ø = 12 mm reinforcing steel segments of 100 mm length have been created using a core drill. Electrical connections have then been established by welding wires on the cut surfaces of the reinforcement and the isolated coupon respectively. Two additional drill holes were

prepared for the placement of the $MnO_2$-reference electrode (type "ERE-20" from Force Technology) and a PT-1000 temperature sensor. Finally, a slot was prepared for the placement of the counter electrode (CE) made of a 20 mm × 120 mm Ti/MMO mesh ribbon (HISEO® Mesh ribbon 20 mm; Chemical Newtech SpA). The reference and the counter electrodes were embedded using a cementitious grout of high electric conductivity (Master-Protect 815 CP from Master Builders Solution GmbH) as shown in Figures 2–4.

## 4.2 | Measurement program

The measurement program was as follows:

1. An interval of 7 days was set up for the coupon to be connected and isolated from the reinforcement (6 days connected, 1 day isolated).
2. In the connected phase the coupon potential, the reinforcement potential, the galvanic current between coupon and reinforcement as well as the concrete temperature were measured every hour.
3. In the disconnected phase, the coupon potential and the reinforcement potential were measured at an interval of 15 min. The first values (instant-off values) were taken 0.5 s after disconnecting the reinforcement from the coupon.
4. At the end of the disconnected phase, an LPR measurement was performed on the disconnected coupon using the embedded counter and reference electrode.
5. Data for precipitation and atmospheric temperature from a weather station 3.5 km away from the car park are included to demonstrate the influence of the ambient environment.

The measurements were performed using the monitoring system "Camur-II" (Protector a.s.).

## 4.3 | Temperature measurements

The temperature of the concrete surrounding the segmented reinforcement was measured using the embedded PT1000 sensor. In addition, the ambient atmospheric temperature was taken from a weather station located approximately 3.5 km away from the subterranean car park 20 cm above ground in the open atmosphere as well as the amount of daily precipitation.

## 4.4 | Potential measurements

Potential measurements were carried out using the embedded reference electrode (RE) both for the coupon and for the reinforcement. Potentials were measured when the circuit between the coupon and the reinforcement was closed and open. When the circuit was closed the ZRA was measuring galvanic current flowing between the coupon and the reinforcement. After disconnecting the coupon from the reinforcement both the coupon and reinforcement potentials were

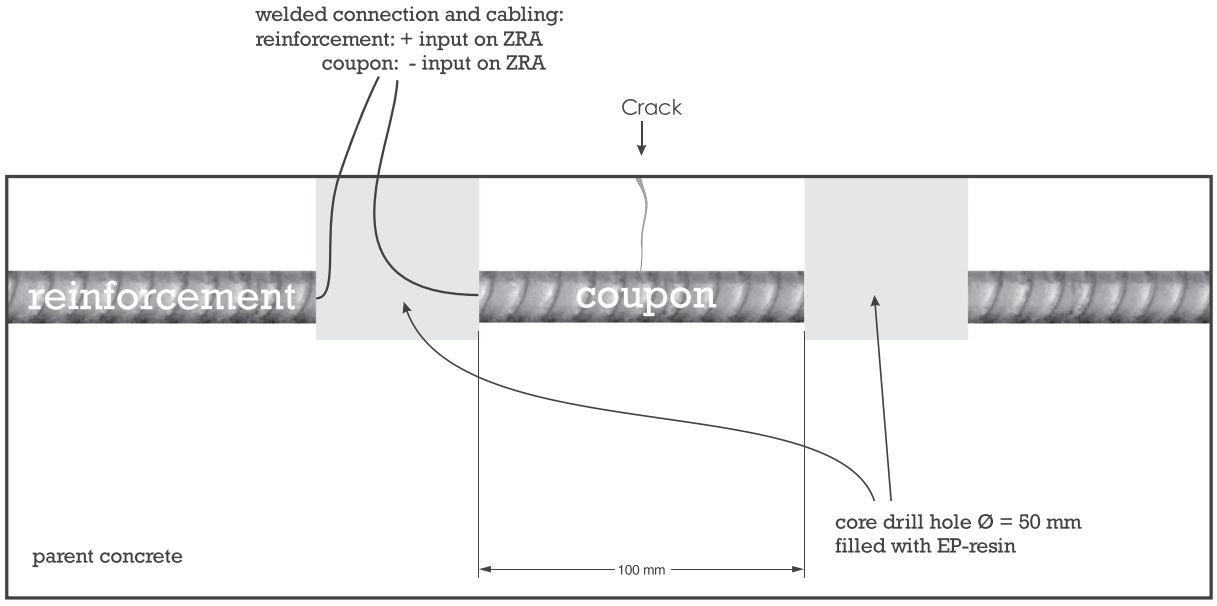


FIGURE 2 Isolating the coupon from the reinforcement and attaching the cables.

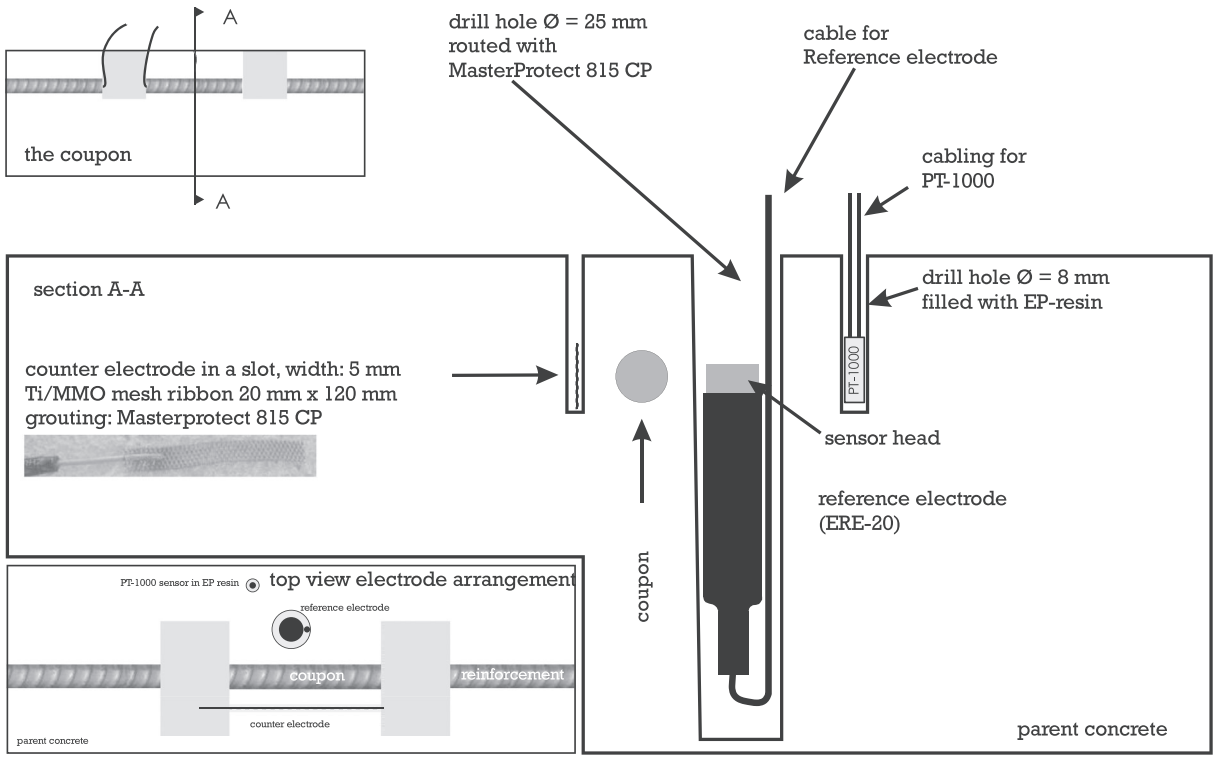


**FIGURE 3** Instrumenting with a reference electrode, a counter electrode and a temperature sensor.

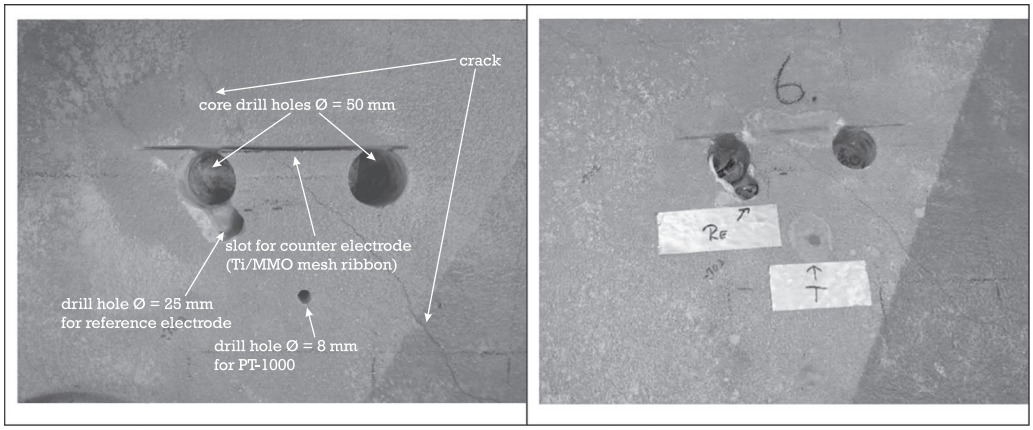


**FIGURE 4** Actual preparation work in the intermediate ceiling of the car park. In the right image the sensors are already in place. Cabling is performed on the underside of the ceiling.

depolarizing in opposite direction. The potential difference measured after 24 h depolarization is in this work considered the driving force of the macro cell even though the depolarization may not be complete after 24 h in every case. A typical development for the coupon and reinforcement potentials at the time regime of a depolarization shows in Figure 5. It also includes the galvanic current density related to the coupon surface (Figure 6).

## 4.5 | Galvanic current measurements

The technique of galvanic current measurements allows to measure the macro-element current of a net anodic portion of the rebar system to a net cathodic portion. The crux is to identify an anodic segment of the reinforcement on an extended reinforcement network. In the present case, the anodic part of the reinforcement was estimated to be located in the vicinity of a crack crossing the reinforcement (see

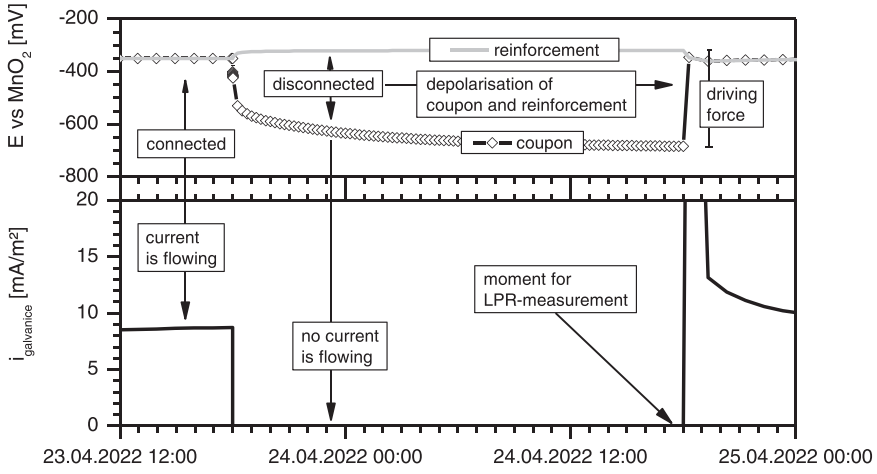


FIGURE 5 Development of the coupon and the reinforcement potential as well as the galvanic current density before and after the coupon was disconnected from the reinforcement.

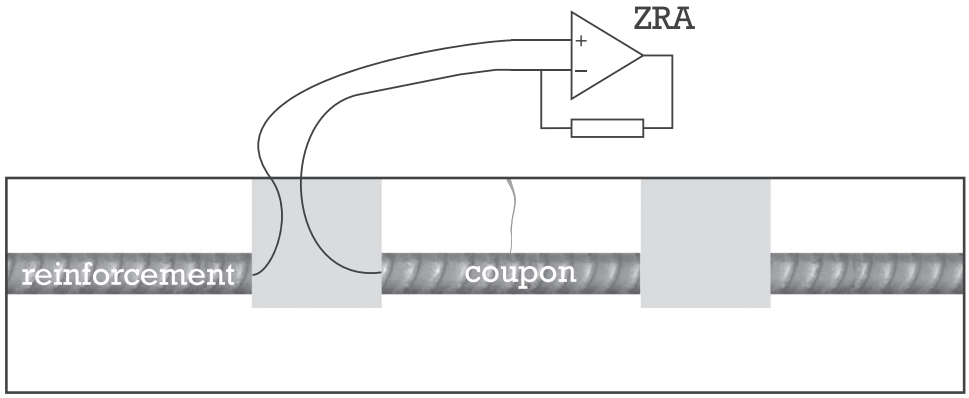


FIGURE 6 Connecting the zero resistance ammeter (ZRA) to a coupon.

Figure 3). Most of the nine isolated coupons were anodic with respect to the remaining reinforcement network, but some were also cathodic.

The galvanic current was measured using an electronic component of the Camur-II system based on the technique of zero resistance ammeter (ZRA). Generally, the negative input on the ZRA was used for the coupon and the positive one for the reinforcement. In this arrangement, the measured current is positive when the coupon is anodic with respect to the reinforcement and negative when the coupon is cathodic. The (positive) coupon current can then be interpreted as the corrosion rate caused by galvanic coupling.

## 4.6 | LPR measurements

The technique relies on the observation that in a potential region near the free corrosion potential the dependence of the current response on the overpotential of a corroding electrode is approximately linear and that the slope of this response (LPR) is inversely proportional to the rate of the corrosion process. LPR measurements of steel in concrete are usually performed using a three-electrode arrangement, comprising the test electrode (rebar), a reference electrode (a half cell) and a counter electrode ("inert" Ti/MMO or similar). The potential of the test electrode is measured with respect to the reference electrode and the test electrode is then polarized by a current from an external source via the counter electrode.

Stern and Geary found that for small perturbations of the potential around the corrosion potential the corrosion current density is proportional to the applied current density divided by the potential shift which is the reciprocal of the polarization resistance $R_P$.[5]

The polarization resistance is thus defined as the slope of the current density-potential relationship at $E_{corr}$.

$$R_P = \left(\frac{dE}{di}\right)_{E_{corr}}, \tag{9}$$

where $dE$ is the potential change (polarization) and $i$ the current density applied.

The relationship between the $i_{corr,LPR}$ and $R_P$ is known as the "Stern-Geary" relationship[6]

$$i_{\text{corr,LPR}} = \frac{B}{R_{\text{P}}}. \tag{10}$$

For the practical applicability of determining corrosion rates from measured polarization resistances, it is important that the quantity $B$ for activation-polarization is almost constant. However, this is usually not the case since quantity $b$ is dependent on the values for the anodic and cathodic Tafel-slopes $b_{\text{a}}$ and $b_{\text{c}}$. The Stern-Geary relationship in its general form is thus given by

$$\frac{1}{R_{\text{P}}} = i_{\text{corr}} \cdot \left( \frac{2.3}{b_{\text{a}}} + \frac{2.3}{b_{\text{c}}} \right). \tag{11}$$

For steel in concrete, the measured values for the anodic Tafel-slopes vary from $1.0 \times 10^{-12}$ to 1.570 V/dec. and for the cathodic Tafel-slopes from 0.01 to 1.250 V/dec.[7]

However, in the present case, the concrete and its exposure is similar for all measurement locations. Therefore, it is assumed that the amount "$B$" is comparable for all measurements carried out in this work and converting the measured polarization resistances into corrosion current densities is therefore justified. Furthermore, the relative changes in the corrosion rates determined by LPR are of major interest.

The shape of a polarization curve of a corroding metal generally depends on the procedure that has been adopted to perform the electrochemical measurements. In particular, when a polarization curve is repeated for several cycles between the values $E_{\text{corr}} + \Delta E$ and $E_{\text{corr}} - \Delta E$, it can be observed that the arches belonging to the anodic or the cathodic zone are not superimposed and the area of the region bounded by two consecutive curves depends on the potential sweep rate.[8]

By plotting the current versus the potential in an $I$–$E$ diagram, a deformed parallelogram is obtained with a slope at the beginning of each potential excursion, equal to $1/R_{\text{el}}$ and equal to $1/(R_{\text{el}} + R_{\text{P}})$ for longer times according to González et al.[9] (see Figure 7).

The apparent polarization resistance $R_{\text{app}}$ is equal to the slope of the polarization curve at the endpoint of one semicycle

$$R_{\text{app}} = \left( \frac{\partial E}{\partial i} \right)_{E_{\text{corr}} \pm \Delta E_{\text{max}}}, \tag{12}$$

where $\Delta E_{\text{max}}$ should not exceed ±20 mV to keep the above relationship linear.

Evaluation of $R_{\text{app}}$ delivers values more close to the true polarization resistance than evaluation of the so-called diagonal resistance $R_{\text{D}}$ which is—according to Macdonald[10]—the gradient of the line joining the endpoints of the voltammogram as shown in Figures 8 and 10. The principal procedure to perform LPR measurements by applying potentiostatic steps is described elsewhere.[11]

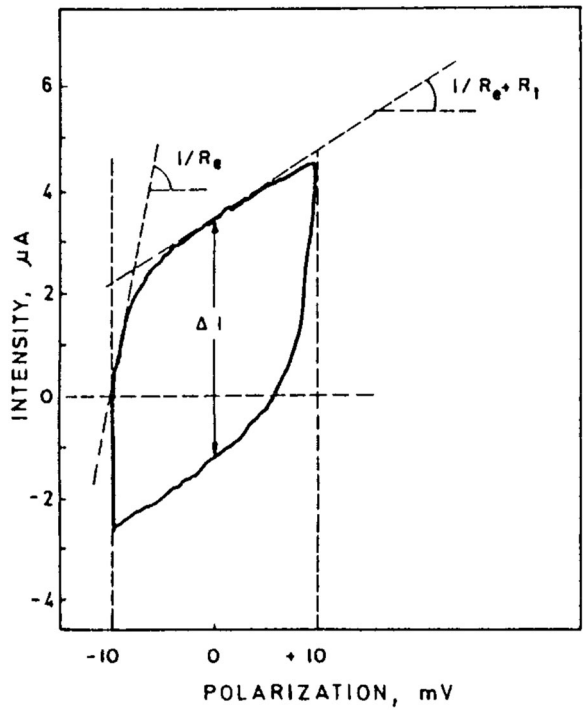


FIGURE 7 Response of a corroding system to a triangular wave of potential (from Rocchini[8]).

Compensation for the IR-drop was not considered being a serious problem, since the reference cell was placed opposite to the counter electrode. The current lines are far less established, there causing a less strong electric field between the reference cell and the rebar to be measured (see Figure 9). The current around the rebar ($I_\theta$) related to the current of the area facing the counter electrode ($I_{\text{max}}$) is according to Feliu et al.[12] given as (Figure 9)

$$\frac{\text{I}_\theta}{\text{I}_{\text{max}}} = \frac{(1-b)^2}{1 - 2b \cdot \cos\theta + b^2}, \tag{13}$$

with: $b = \frac{d}{r} - \sqrt{\frac{d^2}{r^2} - 1}$.

Using a typical rebar diameter (12 mm) and a typical distance of the counter electrode from the steel (10 mm) the distribution of the current around the rebar as a function of the angle $\theta$ is as shown in Figure 9. The current on the opposite side of the steel is only half of the side facing CE. The IR-drop between RE and WE is therefore maximum half of the value that would be obtained when the reference electrode is located at the same side of the steel as the counter electrode.

In this work, LPR measurements have been carried out in the following way

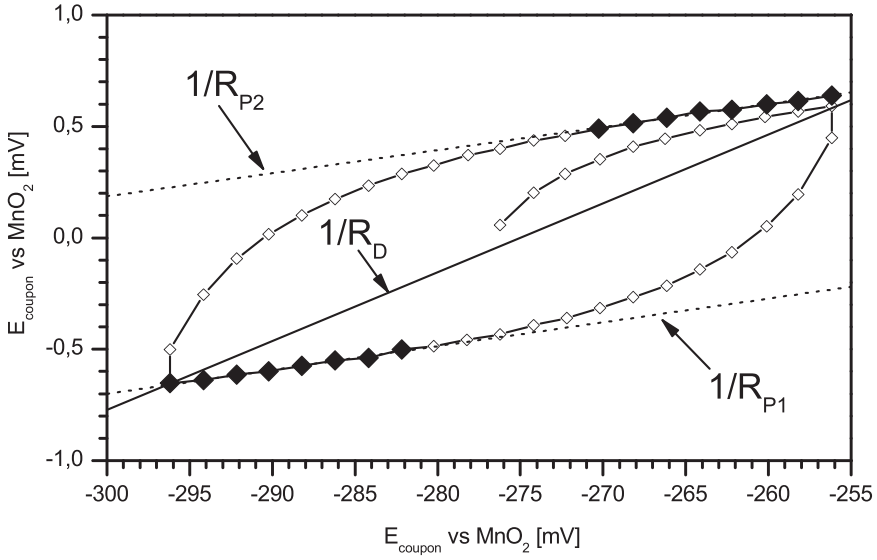


**FIGURE 8** Evaluation of (potentiostatic) linear polarization resistance measurements in this work.

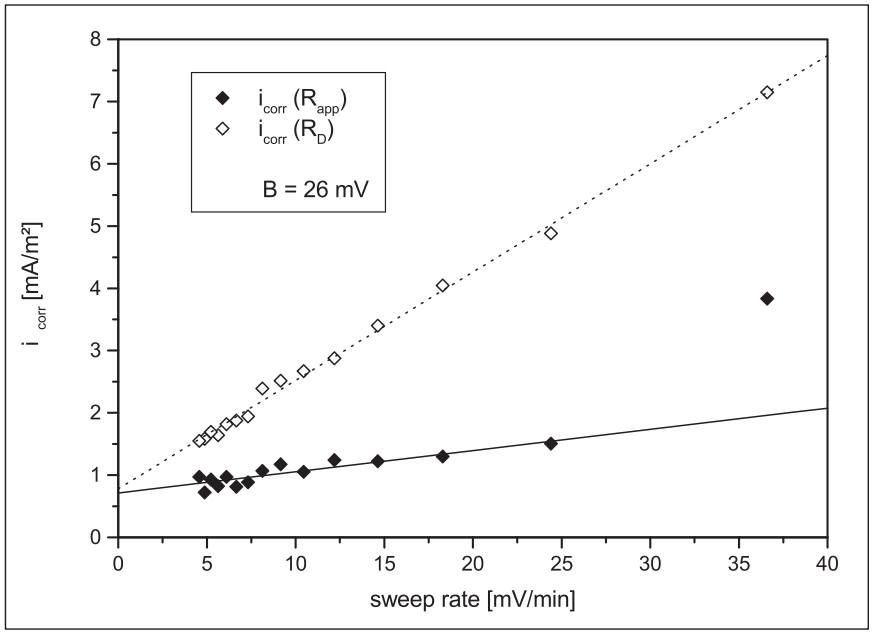


**FIGURE 9** Dependence of the measured $i_{corr}$ calculated from $R_D$ and $R_{app}$ determined at various sweep rates using Equation (10) (from Pruckner[11]).

Starting at the corrosion potential, small potential steps (2 mV every 20 s) have been applied until a polarization $\Delta E$ of +20 mV was reached, then the working electrode (WE) has been polarized in steps again until a polarization $\Delta E$ of −20 mV was reached and again back to a polarization of $\Delta E$ of +20 mV.

The data set resulting (potential/current density) was treated as described in Figure 8 to obtain the closest value of $R_{app}$ to the true value for the polarization resistance $R_{P,true}$ and its standard deviation

$$R_{app} + \sigma_D(R_{app}) = \frac{R_{P1} + R_{P2}}{2} \pm \sqrt{\left(R_{P1} - \frac{R_{P1} + R_{P2}}{2}\right)^2 + \left(R_{P2} - \frac{R_{P1} + R_{P2}}{2}\right)^2}. \quad (14)$$

The standard deviation for the corrosion current density is calculated accordingly

$$i_{corr,LPR} + \sigma_D(i_{corr,LPR}) = \frac{B}{2} \cdot \frac{R_{P1} + R_{P2}}{R_{P1} \cdot R_{P2}} \pm \sqrt{\left(\frac{B}{R_{P1}} - \frac{B}{2} \cdot \frac{R_{P1} + R_{P2}}{R_{P1} \cdot R_{P2}}\right)^2 + \left(\frac{B}{R_{P2}} - \frac{B}{2} \cdot \frac{R_{P1} + R_{P2}}{R_{P1} \cdot R_{P2}}\right)^2}. \quad (15)$$

When $R_{P1}$ and $R_{P2}$ do not differ significantly, the system can be considered being in a stationary condition and/or that the measurement resolution is sufficiently high. As a measure for the reliability of the obtained

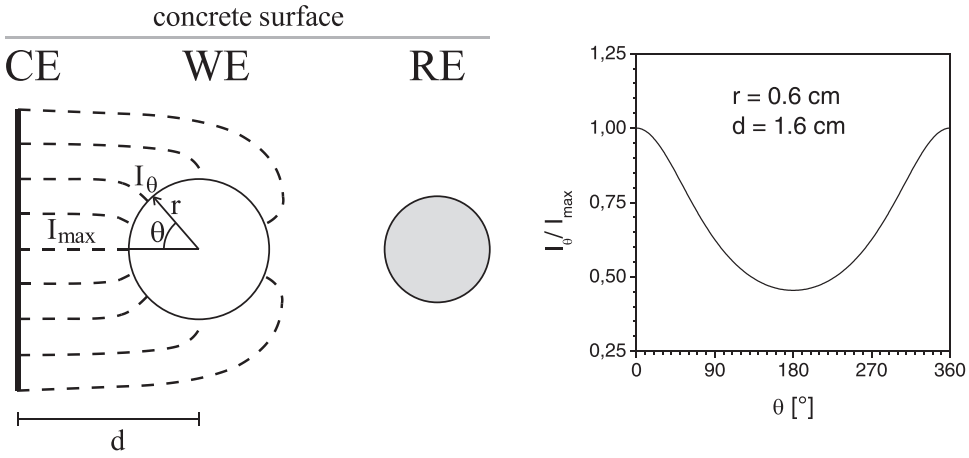


**FIGURE 10** Schematic current lines between counter electrode and reinforcing steel (left) and ratio of the current absorbed by the steel at location θ to the location facing the counter electrode (right). CE, counter electrode; RE, reference electrode; WE, working electrode.

polarization resistance serves as the standard deviation of the mean value for $R_{P1}$ and $R_{P2}$. When corrosion current densities are presented then the standard deviation according to Equation (15) is used.

While $i_{corr,LPR}$ calculated from $R_{app}$ is close to the true value using the "diagonal resistance" $R_D$ values for $i_{corr,LPR}$ are obtained that differ much more from the true value and increase much faster with the sweep rate.

## 5 | RESULTS AND DISCUSSION

The measurements have been carried out over a period of approximately 1 year. The measurements are shown for three locations in the subterranean car park:

MST-1, parking bay in the first basement level,
MST-7, driving lane in the third basement level,
MST-9, driving lane in the third basement level.

Figures 11 and 12 show the development of the concrete temperature at location MST-1 and MST-9 in the top diagrams as well as the ambient atmospheric temperature taken at the weather station located approximately at a distance of 3.5 km to the subterranean car park. In the middle diagrams, the development of the coupon and reinforcement potentials with time are pictured and in the bottom diagrams the galvanic current densities related to the coupon surfaces.

The vertical lines in the potential and current diagrams of Figures 11 and 12 are caused by the periodic disconnection of the coupons from the reinforcement and resolve as in Figure 5 when zooming into the time scale.

Figures 13 and 14 show the galvanic current densities immediately before disconnecting the segmented coupons from the reinforcement, as well as the corrosion current densities measured at the end of the disconnected phase together with concrete and ambient atmospheric temperature for the locations MST-1 and MST-9. While for location MST-1 the obtained corrosion current density is around 5 mA/m² coupon surface and in similar range as the galvanic current density the corrosion current density at MST-9 is one order of magnitude less and the galvanic current density reaches negative values after some time indicating the coupon becoming slightly more noble than the reinforcement.

The variation of the galvanic current density is usually more pronounced than the corrosion current density and it can be higher or lower than the corrosion current density and it can also take negative values as discussed in paragraph 2 (Section 2). This clearly shows in Figures 13, 14, and 17.

From the depolarization of the coupon and the reinforcement after disconnecting them, a series of parameters may be obtained. The depolarization of the coupon within approximately 0.5 s divided by the galvanic current can be considered as the spread resistance of the coupon, the 24-h depolarization of the coupon (from 0.5 s to 24 h) divided by the galvanic current as a polarization resistance of the coupon. Finally, the potential difference between coupon and reinforcement after 24 h depolarization as the driving force of the macrocell consisting of coupon and reinforcement. Figures 15 and 16 show the IR-drop of the coupon ($\Delta E_{iR,coupon}$) the 24-h depolarization value of the coupon ($\Delta E_{24\text{-h depol,coupon}}$) and the

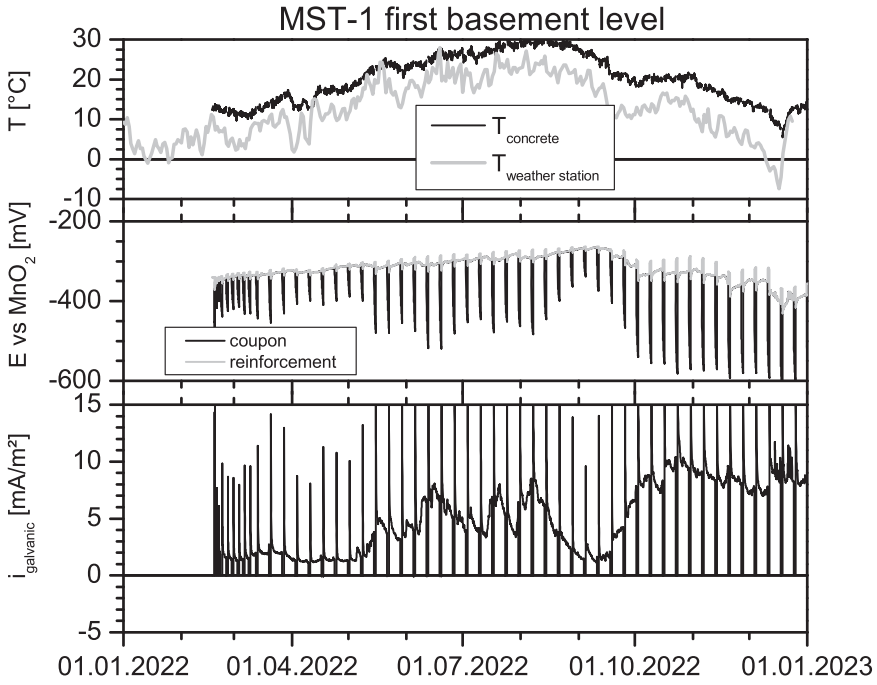


**FIGURE 11** Presentation of concrete and ambient atmospheric temperature, coupon and reinforcement potentials and galvanic currents for the location MST-1.

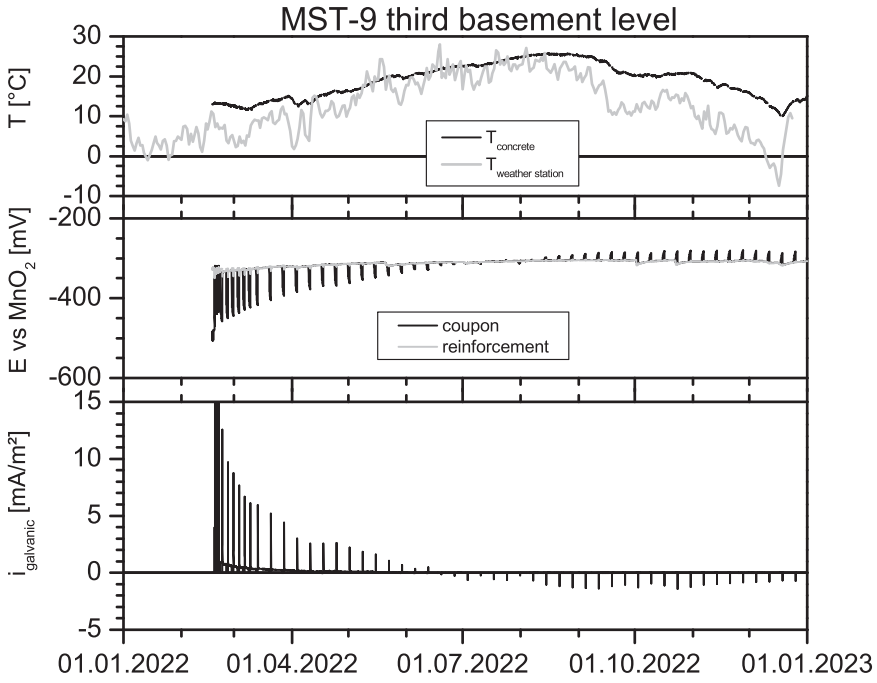


**FIGURE 12** Presentation of concrete and ambient atmospheric temperature, coupon and reinforcement potentials and galvanic currents for the location MST-9.

driving force of the macrocell ($\Delta U_{\text{circuit}}$) with time for the location MST-1 and MST-9. The driving force of the macrocell at MST-9 was reaching up to 300 mV. The driving force for the macrocell MST-9 became negative with time which means that the coupon turned cathodic compared with the reinforcement and corrosion of the coupon due to galvanic coupling stopped.

On the location MST-7 obviously precipitation caused a sudden increase in both the galvanic current density of the coupon as well as in the corrosion current density of the same determined by LPR (Figure 17). A period of 6 days (November 15, 2022 to November 20, 2022) can be attributed to the eightfold increase of the galvanic current density and a twofold increase of the corrosion current density as shown in Figure 17. The temperature

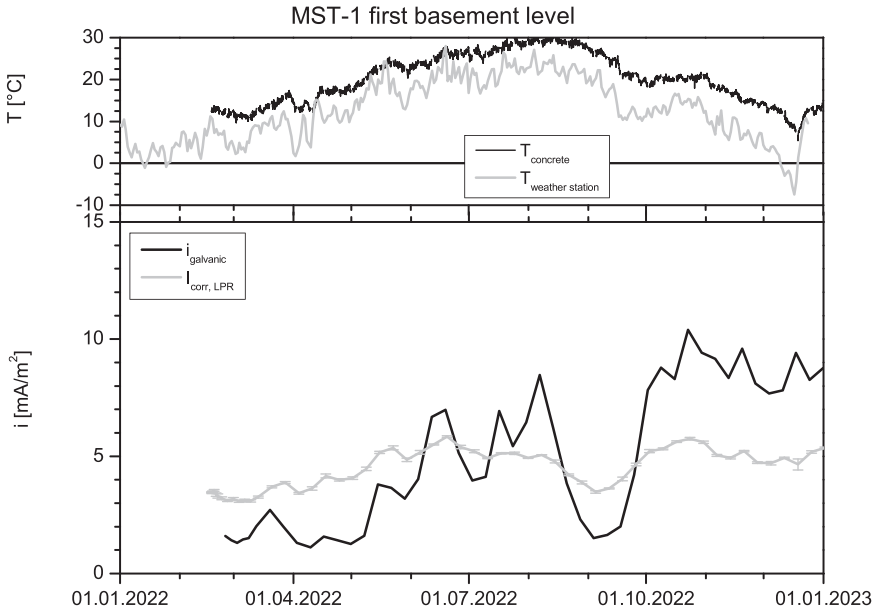


**FIGURE 13** Galvanic and corrosion current density as well as concrete and ambient atmospheric temperature for the location MST-1.

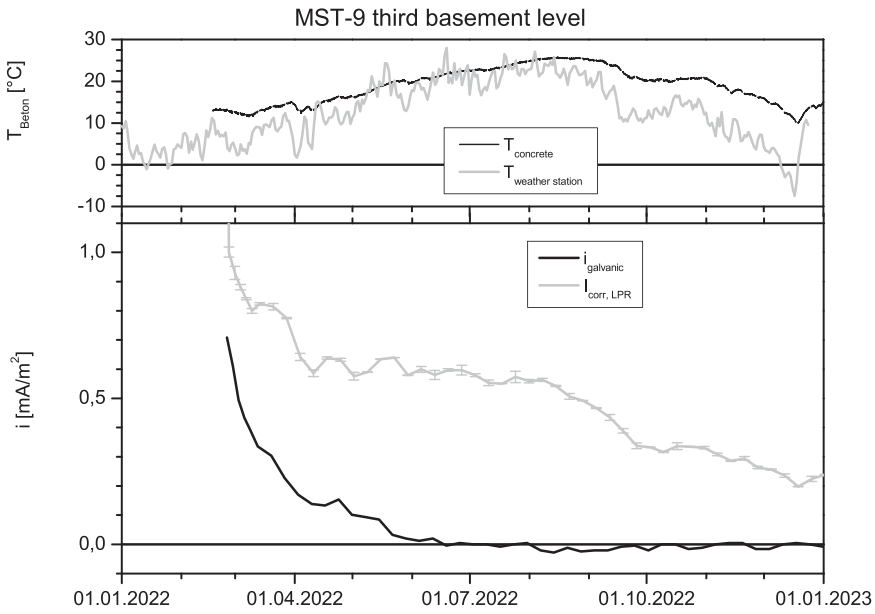


**FIGURE 14** Galvanic and corrosion current density as well as concrete and ambient atmospheric temperature for the location MST-9.

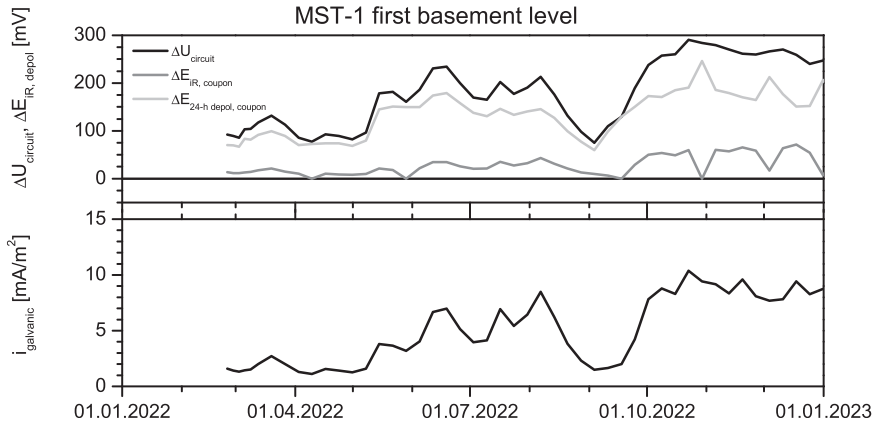


**FIGURE 15** IR-drop and 24-h depolarization value of the coupon and driving force as well as galvanic current with time for the location MST-1.

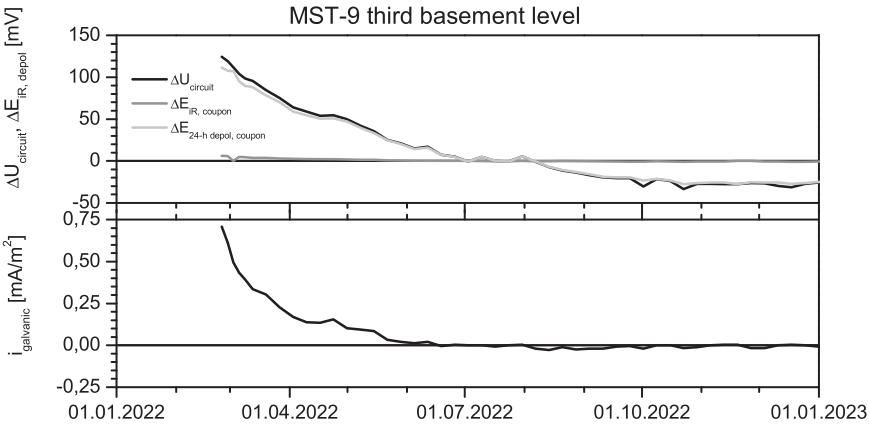


**FIGURE 16** IR-drop and 24-h depolarization value of the coupon and driving force as well as galvanic current with time for the location MST-9.

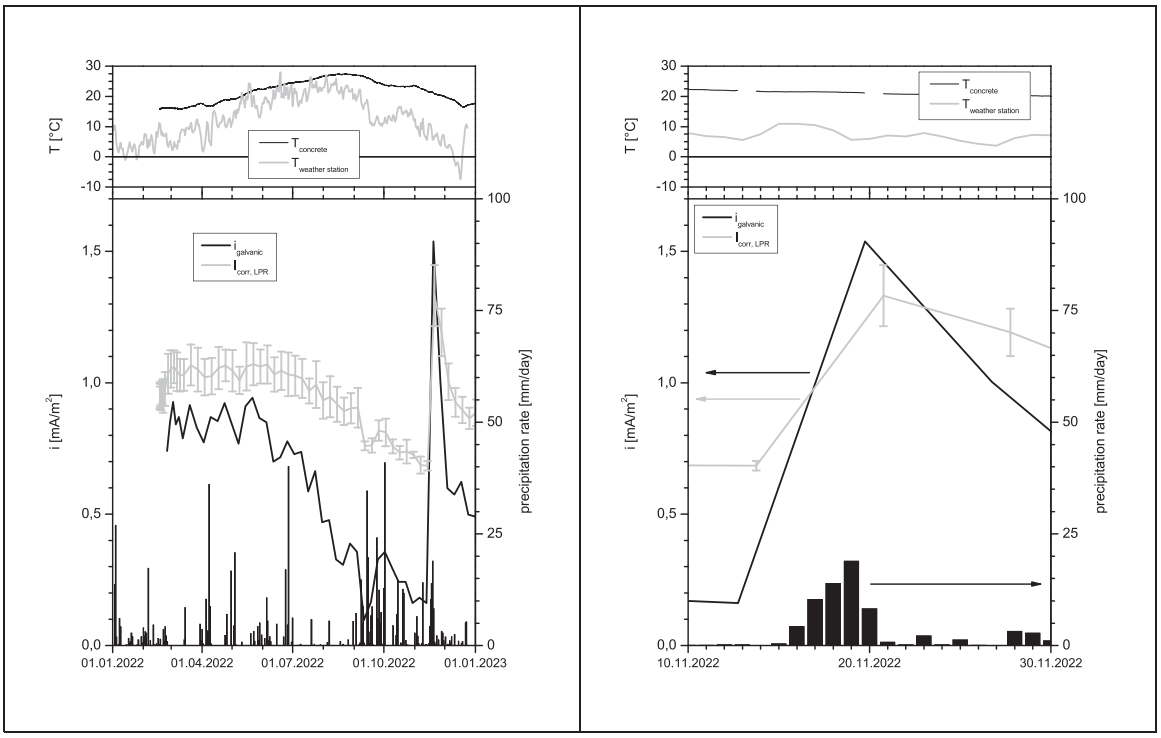


**FIGURE 17** Development of the galvanic and corrosion current density with time together with the concrete and ambient temperature as well as the daily precipitation at location MST-7.

variation in this period would be far too small to cause such an increase. The increase in the galvanic as well as in the corrosion current density was, however, not sustainable. The values for the galvanic and corrosion current density were dropping within days close to the values before water ingress happened.

For the location (MST-1) it was less obvious that the change of the corrosion current density was caused by water ingress. In this case, the measured corrosion current density was corrected for the temperature effect. To distinguish between corrosion current changes due to changes in the concrete temperature and due to changes in the electrolyte surrounding the coupon (i.e., water ingress due to precipitation) the corrosion current densities on location MST-1 were standardized to 298 K using Arrhenius' law (Equation 8). For the location MST-1 a value of EA = 27.5 kJ/mol fits best to minimize the temperature-caused perturbation of the corrosion current transient. It can be clearly shown that the measured variations in corrosion current density until beginning of September 2022 were mainly caused by temperature variations whereas the increase in the standardized corrosion current density obviously was caused by moisture ingress as a consequence of the increased precipitation rate starting in September 2022 (Figure 18).

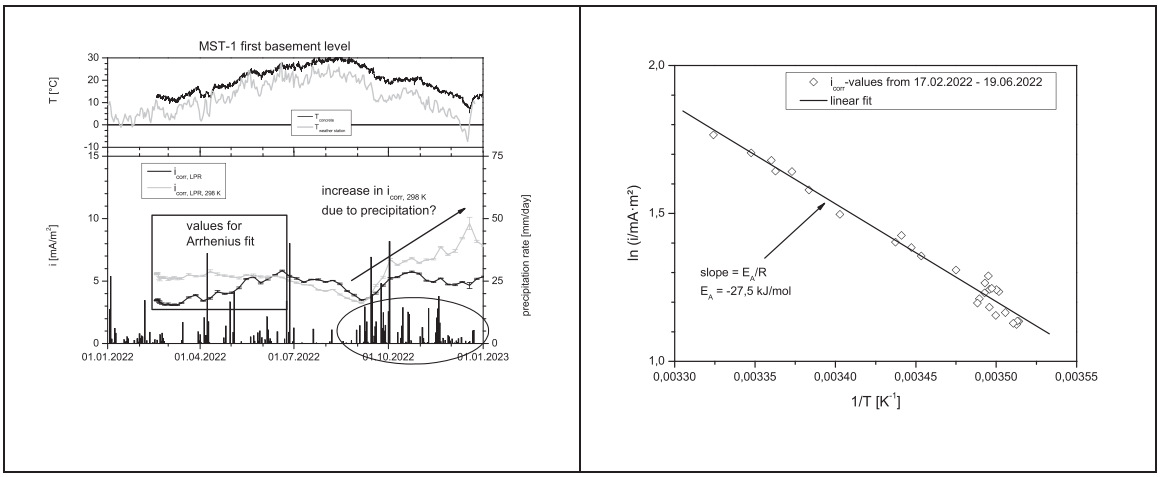


**FIGURE 18** Development of the corrosion current density with time together with the concrete and ambient temperature as well as daily precipitation. The cyan line is the standardized corrosion current density using Arrhenius' law (Left). The values from 17.02. to 19.06.2022 were used for fitting Arrhenius' law to the corrosion current density (right).

## 6 | CONCLUSIONS

1. It could be shown that measurements of galvanic currents and corrosion currents and thereof calculating $i_{galvanic}$ and $i_{corr,LPR}$ can be performed together on a segmented reinforcement. Disconnecting the segment from the reinforcement also allows the determination of the driving force $\Delta U_{circuit}$ for the macrocell and the determination of the corrosion current density on the nonpolarized segment of the reinforcement.
2. The chosen technique of LPR measurement allows the determination of the polarization resistance close to the true value.
3. $i_{corr,LPR}$ is in a similar range as $i_{galvanic}$. However, for from the reinforcement segmented coupons the galvanic current may be higher than $i_{corr,LPR}$, lower than $i_{corr,LPR}$ or even negative.
4. The corrosion current density is influenced by environmental parameters. A correction for the temperature dependence using the electrochemical Arrhenius relation may let changing environmental conditions—other than temperature—that influence the corrosion rate become more pronounced in a corrosion current or galvanic current versus time presentation.

### ACKNOWLEDGMENTS

The operator of the car park (Stadtwerke Heidelberg Garagen GmbH) and his consultant (Ingenieurgruppe Bauen PartG mbB) enabled the installation and the use of the measured data. The carefully performed installation by instakorr GmbH and financial support of the project by Master Builder Solutions Deutschland GmbH is gratefully acknowledged.

### DATA AVAILABILITY STATEMENT

Research data are not shared.

### ORCID

*Franz Pruckner* http://orcid.org/0009-0006-5260-9469

### REFERENCES

[1] C. Wagner, W. Traud, *Z. Elektr.* **1938**, *44*, 391.
[2] S. E. Benjamin, J. M. Sykes, *Arab. J. Sci. Eng.* **1995**, *20*, 269.
[3] F. Pruckner, presented at *CONSEC. 98*, Tromsø, Norway, 21–24 June, **1998**. 519.
[4] R. R. Hussain, *Int. J. Electrochem. Sci.* **2012**, *7*, 3656.
[5] M. Stern, A. L. Geaby, *J. Electrochem. Soc.* **1957**, *104*, 56.
[6] E. Heitz, W. Schwenk, *Werkst. Korros.* **1976**, *27*, 1976.
[7] E. Garcia, J. Torres, N. Rebolledo, R. Arrabal, J. Sanchez, *Materials* **2021**, *14*, 2491.
[8] G. Rocchini, *Corros. Sci.* **1994**, *36*, 1063.
[9] J. A. González, A. Molina, M. L. Escudero, C. Andrade, *Corros. Sci.* **1985**, *25*, 917.
[10] D. D. Macdonald, *J. Electrochem. Soc.* **1978**, *125*, 1443.
[11] F. Pruckner, *PhD Thesis*, University of Vienna (Austria), **2001**.
[12] S. Feliu, J. A. González, C. Andrade, *Corrosion* **1995**, *51*, 79.

**How to cite this article:** F. Pruckner, *Mater. Corros.* **2023**, 1.
https://doi.org/10.1002/maco.202313894